JOURNAL OF MATERIALS SCIENCE 31 (1996) 4697–4704

The toughening behaviours of Cr_3C_2 particulate-reinforced Al_2O_3 composites

CHEN-TSU FU, AI-KANG LI
Material Research Laboratories, Industrial Technology Research Institute, Hsinchu, 31015, Taiwan

Enhancement of the fracture toughness of Al_2O_3 was achieved by the additions of 10–40 vol% Cr_3C_2 particulates through a hot-pressing process. The dependence of Cr_3C_2 particle size (0.5, 1.5 and 7.5 μm) on the toughening effect was investigated. The maximum fracture toughness of composites could be improved to 5.9, 7.6 and 8.0 MPa $m^{1/2}$ for fine, medium and coarse Cr_3C_2 particle reinforced composites, respectively. Both the quantitative analysis of toughening contributions and experimental observations are extensively discussed in terms of Cr_3C_2 particle size, microcracks, as well as thermal residual stress between Al_2O_3 and Cr_3C_2.

1. Introduction

During the last few years, several primary toughening mechanisms of particulate-reinforced ceramics have been attributed to (i) interaction between the crack front and particles (e.g. crack-bowing model) [1, 2], (ii) crack deflection by particles at the front of propagating cracks [3, 4], (iii) crack bridging by strong or ductile particles [5–7], (iv) residual stress (strain) field due to mismatch between the coefficients of thermal expansion or Young's modulus of the ceramic matrix and particulates [8, 9], (v) the incidence of microcracking to form a process zone around the macrocrack tips [10–12], and (vi) matrix grain bridging [7, 13, 14]. In previous studies [1, 3–5, 8, 14], a unique toughening mechanism was only quantitatively proposed in a composites system, but it is noted that the aforementioned toughening mechanisms may be highly interactive and may take place simultaneously in the composite [15, 16]. Thus, it may be extremely difficult, either analytically or experimentally, to determine the individual contributions. However, the guideline and interactions noted should be useful in material design and improvement.

Recently, although the dependence of particle size of the reinforcements on the toughness of ceramic particulate composites has been investigated [15–17], the microstructural evolution, e.g. microcracks, residual stress and interfacial bonds between reinforcements and matrix, still do not show any clear particle-size dependence. However, it is well documented that the microstructure of ceramics plays a very important role in mechanical properties for monolithic ceramics [18] and whisker composites [13].

In this study, an attempt was made to investigate the correlations between microstructure and fracture toughness of 10–40 vol% Cr_3C_2 particulate-reinforced Al_2O_3 matrix composites with three Cr_3C_2 particle sizes. Meanwhile, the individual contributions of the common toughening mechanisms are also quantitatively studied and related to the dependence of particle size and content of Cr_3C_2 reinforcements. The details of sintering behaviour, oxidation resistance as well as feasibility of electrical-discharge machining (EDM) of the Al_2O_3–Cr_3C_2 composites, were reported elsewhere [19, 20].

2. Experimental procedure

2.1. Raw materials

The Cr_3C_2 particles used in this investigation were Herman C. Stark's product (grade A) and purity higher than 99%. There are three particle sizes of the Cr_3C_2 powders. The mean particle size, measured by laser diffraction techniques, are 7.5 μm (L), 1.5 μm (M) and 0.5 μm (S), respectively. The finest particle was obtained by attrition milling the 1.5 μm particle for 48 h. The Al_2O_3 powder was Alcoa's product (A16-SG) with particle size 0.3–0.5 μm and a purity is higher than 99.7%.

2.2. Consolidation procedures

At first, Al_2O_3 with 10–40 vol% Cr_3C_2 powders were added, together with deionized water, and then ball-milled for 24 h. The slurry was further homogenized for 15 min using a high shear ultrasonic dispersing process. The homogenized slurry was dried rapidly with constant agitation on a hot plate. Dried and sieved mixture was uniaxially pre-pressed to form discs, 5 mm high and 60 mm diameter. The green compacts were then placed in a boron nitride-coated graphite mould and hot-pressed at 1400 °C in an argon atmosphere, under a pressure of 30 MPa for 1 h.

0022–2461

2.3. Characterization

The dense composite discs were ground and cut, along the grinding direction, into 3 mm × 4 mm × 40 mm bars. The fracture toughness was evaluated using the single-edge-notched beam (SENB) method and measured at room temperature. Each bar to be used for fracture toughness tests, was centre-notched to one-third of its thickness using a 0.15 mm thick diamond blade. The microstructures of Al_2O_3/Cr_3C_2 composites were examined by scanning electron (SEM) and transmission electron (TEM) microscopes.

The Al_2O_3 grain size was evaluated by the line intercept method after the samples were chemically etched in hot phosphoric acid.

3. Results and discussion

3.1. Microstructural development and formation of microcracks

Cr_3C_2 particulate-reinforced Al_2O_3 composites can be hot-pressed to obtain a density greater than 98.5% theoretical at 1400 °C, and hence a flexural strength higher than 600 MPa [19].

The scanning electron micrograph of the polished surface of dense Al_2O_3–30 vol % Cr_3C_2 (M) composites sintered at 1400 °C is shown in Fig. 1. The particle size of Cr_3C_2 for the composites sintered at 1400 °C was about 2 μm shown in Fig. 1, and every close to the size of the raw Cr_3C_2 particles.

The transmission electron micrographs of dense Al_2O_3–10 vol % Cr_3C_2 composites sintered at 1400 °C with three particle sizes of Cr_3C_2 powder (0.5, 1.5 and 7.5 μm) are shown in Fig. 2a–c, respectively. The locations of fine Cr_3C_2 particles (S) were either at the boundary or embedded in the matrix grain, as shown in Fig. 2a. When the coarser Cr_3C_2 powders were used, e.g. 1.5 and 7.5 μm, the Cr_3C_2 particle size was equivalent to or larger than the Al_2O_3 grain size and one Cr_3C_2 particle was surrounded by several Al_2O_3 grains. No microcracks were found in any of the Al_2O_3–10 vol % Cr_3C_2 composites. However, several circumferential microcracks, were found to exist at the Al_2O_3/Cr_3C_2 interfaces for Al_2O_3–20 vol % Cr_3C_2 composites reinforced by coarse Cr_3C_2 particles, as indicated in Fig. 2d, while no microcracks were found at the Al_2O_3/Cr_3C_2 interfaces for Al_2O_3–30 vol % Cr_3C_2 composites reinforced by fine or medium Cr_3C_2 particles.

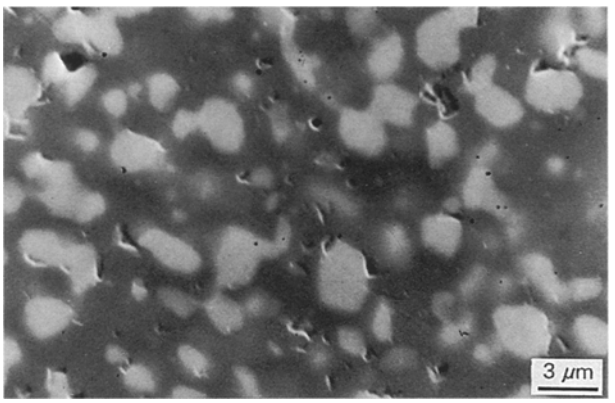

Figure 1 Scanning electron micrograph of Al_2O_3–30 vol % Cr_3C_2 (M) composites hot-pressed at 1400 °C. The white Cr_3C_2 particles are distributed in a grey Al_2O_3 matrix.

There is an important factor, namely the residual stress, which is generated from the large thermal expansion mismatch. The thermal expansion coefficient (TEC) of Cr_3C_2 ($11.2 \times 10^{-6}\,°C^{-1}$) is greater than the TEC of Al_2O_3 ($8.8 \times 10^{-6}\,°C^{-1}$); a quantitative analysis of residual stress resulting from the thermal mismatch in ceramic composites was determined from Equation 1 [21]

$$\bar{\sigma} = \frac{(\alpha_m - \alpha_p)\Delta T}{(1 + \nu_m)/2E_m + (1 - 2\nu_p)/E_p} \quad (1)$$

where the subscript m refers to the matrix and p to the particle, E is Young's modulus and ν is Poisson ratio of the materials. Based on Equation 1, the maximum compressive residual stress acting on the Al_2O_3 matrix in the hoop direction is around 1 GPa, but then a tensile residual stress acts on the interface in the radial direction. The value of radial tensile residual stress is higher than the fracture strength of composites (maximum fracture strength is 780 MPa) [19]. So, it is reasonable that the penny-shaped microcracks at the Al_2O_3/Cr_3C_2 interface could be obtained.

There is another quantitative analysis that demonstrated the dependence of particle size of reinforcements on the magnitude and spatial distribution of residual stress, as indicated by Equation 2 [21]

$$\sigma = \bar{\sigma}\frac{R^3}{r^3} \quad (2)$$

where $\bar{\sigma}$ is the residual stress that the spherical particles is subject to uniform hydrostatic stress. This stress is the same as in Equation 1. R is the radius of particulate reinforcements, and r the distance from the centre of the particle ($r \geqslant R$). Based on Equation 2, the magnitude of residual stress is independent of the particle size of reinforcements just at the interface ($r = R$). However, the residual stress induced by larger particles is much higher than that induced by smaller particles as the position in the matrix gradually moves further away from the interface, because the magnitude of residual stress is proportional and inversely proportional to the triple order function of the Cr_3C_2 particle size and the distance from the particle's centre, respectively.

Actually, the occurrence of microcracks in ceramic composites apparently relates to the particle size of the second phase. Based on the stored elastic strain energy converting to work of fracture in materials, Rice [15] and Tsukuma *et al.* [22] proposed that there is a critical particle size, D_s, of second phase beyond which spontaneous microcracking would occur. The critical spherical particle size is determined by several factors, as indicated by Equation 3

$$D_s = \frac{10\gamma_m}{(\Delta\varepsilon)^2 E} \quad (3)$$

where γ_m is the fracture energy for microcracking, $\Delta\varepsilon$ the particle–matrix mismatch strain ($\sim\Delta\alpha\Delta T$; $\Delta\alpha$ is

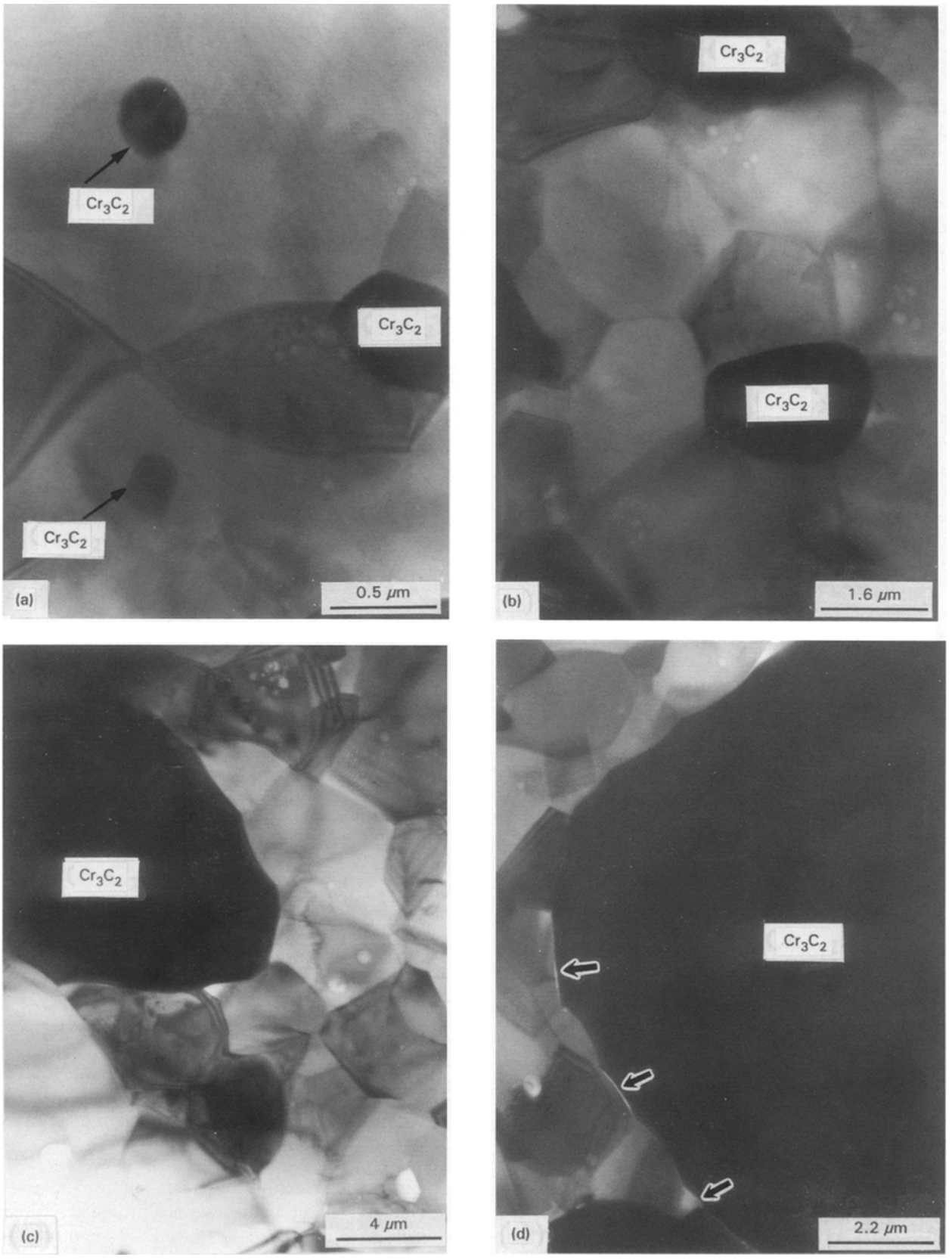

Figure 2 Transmission electron micrographs showing the location of Cr_3C_2 relative to the Al_2O_3 matrix grains in Al_2O_3–Cr_3C_2 composites incorporating three particle sizes, d, of Cr_3C_2 powders and hot-pressed at 1400 °C: (a) 10 vol % Cr_3C_2, $d = 0.5$ μm, arrows indicate the fine Cr_3C_2 particles (< 0.3 μm) are entrapped in Al_2O_3 grains; (b) 10 vol % Cr_3C_2, $d = 1.5$ μm; (c) 10 vol % Cr_3C_2, $d = 7.5$ μm; (d) 20 vol %, $d = 7.5$ μm, arrows indicate the spontaneous microcracks in the presence of Al_2O_3/Cr_3C_2 interfaces.

the thermal expansion mismatch and ΔT is the temperature difference over which the elastic strain builds up), and E is Young's modulus of the matrix material.

Approximate parameters and resultant estimates for D_s in Al_2O_3/Cr_3C_2 composites are shown in Table I. The value of critical Cr_3C_2 particle size of Al_2O_3/Cr_3C_2 composites is about 3.2 μm. This result is very consistent with the microstructural observations, as shown in Fig. 2. While the particle size of Cr_3C_2 is below and close to the critical value, the

TABLE I The approximate parameters and resultant estimates for D_s in Al_2O_3–Cr_3C_2 composites determined by Equation 3

Composite	$\Delta\alpha$ (10^{-6} °C^{-1})	ΔT (°C)	E (GPa)	γ (J m^{-2})	D_s (μm)
Al_2O_3–Cr_3C_2	2.4	1200	365	1	3.2

stress-induced microcracks may be acquired by the contribution of applied stress. Furthermore, it is interesting to note that there seems to exist a critical volume fraction above which spontaneous microcracking will occur and this critical volume fraction is related to the critical particle size [23]. For example, the critical size is > 3.2 μm for $V_f = 0.1$ but is < 3.2 μm for $V_f = 0.2$. There has been no theoretical model or critical particle size that can predict the dependence on the critical volume fraction of second-phase particles, until now. The reason for the dependence on the volume fraction is associated with the tensile residual stress in the composites. Based on the residual stress analysis, it was found that the distribution of tensile residual stress in the matrix will be superimposed and readily resulted in the formation of the spontaneous microcracks, because the content of second phase is high and the distance between particles is short. Therefore, the greater content of reinforcing phases exhibits the higher density of microcracks. Thus, no or little spontaneous microcracking can be found in the Al_2O_3–10 vol % Cr_3C_2 (L) and 30 vol % Cr_3C_2 (M) composites. However, it is easy to observe that the penny-shaped microcracks spontaneously occur in Al_2O_3–20 vol % Cr_3C_2 (L) and the Al_2O_3–40 vol % Cr_3C_2 (M) composites. Otherwise, owing to the small thermal-mismatch of strain, there is no spontaneous microcrack existing in Al_2O_3–40 vol % Cr_3C_2 composites reinforced with fine Cr_3C_2 particles. Thus, based on the microstructural observations, the critical Cr_3C_2 content of Al_2O_3–Cr_3C_2 composites, above which spontaneous microcracking will occur, is 10 and 30 vol % for composites reinforced with coarse and medium Cr_3C_2 powders, respectively.

According to earlier studies [7, 12, 15] on toughening mechanisms for non-transformation ceramic composites, it is very important for the selected reinforcements not to react chemically with the matrix, in order to give high-toughness composites. Therefore, it is necessary to investigate further the possible interfacial reactions in the Al_2O_3–Cr_3C_2 composites system. X-ray diffraction analysis of hot-pressed composites indicated that there was no chemical reaction between Cr_3C_2 and Al_2O_3. A transmission electron micrograph of an interface between Al_2O_3 and Cr_3C_2 is shown in Fig. 3. There is no evidence of a reaction layer existing at the Al_2O_3/Cr_3C_2 interface for composites, as depicted in Fig. 3.

3.2. Fracture toughness

The fracture toughness of the composites is illustrated in Fig. 4 as a function of Cr_3C_2 content. For the medium and coarse Cr_3C_2 particle-reinforced Al_2O_3 composites, the fracture toughness initially increases with Cr_3C_2 content and gives a peak value at 7.5 and 8.0 MPa m$^{0.5}$ for 20 and 30 vol % Cr_3C_2 content, respectively, and then drops slightly, while for the fine Cr_3C_2 particle-reinforced Al_2O_3 composites, the fracture toughness gradually increases with Cr_3C_2 content to 5.9 MPa m$^{0.5}$. The interactions between Cr_3C_2 particles and microcracks induced by the Vicker's indentor have been revealed in Fig. 5a. It is apparent that the primary toughening mechanisms are crack bridging and deflection. Although the toughening mechanism of microcracking which is practically available to Al_2O_3–Cr_3C_2 composites, cannot clearly be observed in Fig. 5a, the other toughening

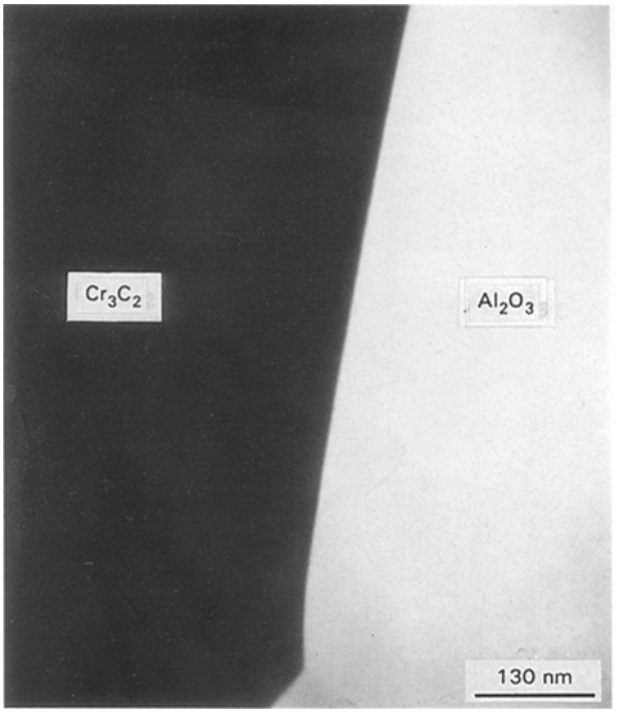

Figure 3 Transmission electron micrograph of the Al_2O_3/Cr_3C_2 interface of Al_2O_3–20 vol % Cr_3C_2 (S) composite hot-pressed at 1400 °C.

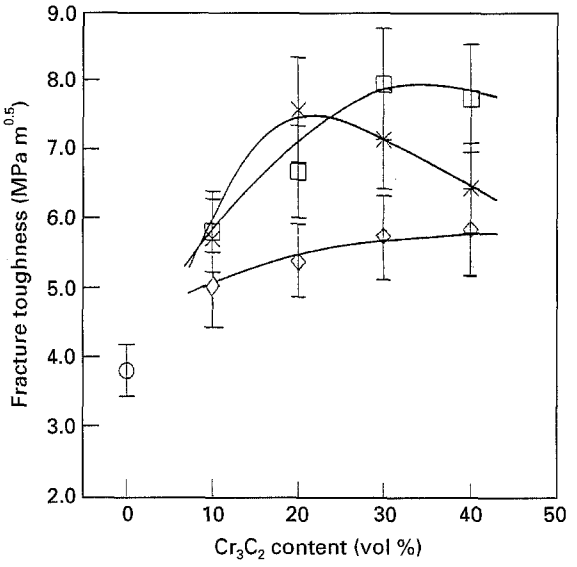

Figure 4 Fracture toughness of Al_2O_3–Cr_3C_2 composites with various contents and particle sizes of Cr_3C_2. (○) Al_2O_3 (◇) 1400 °C, S; (×) 1400 °C, M; (□) 1400 °C.

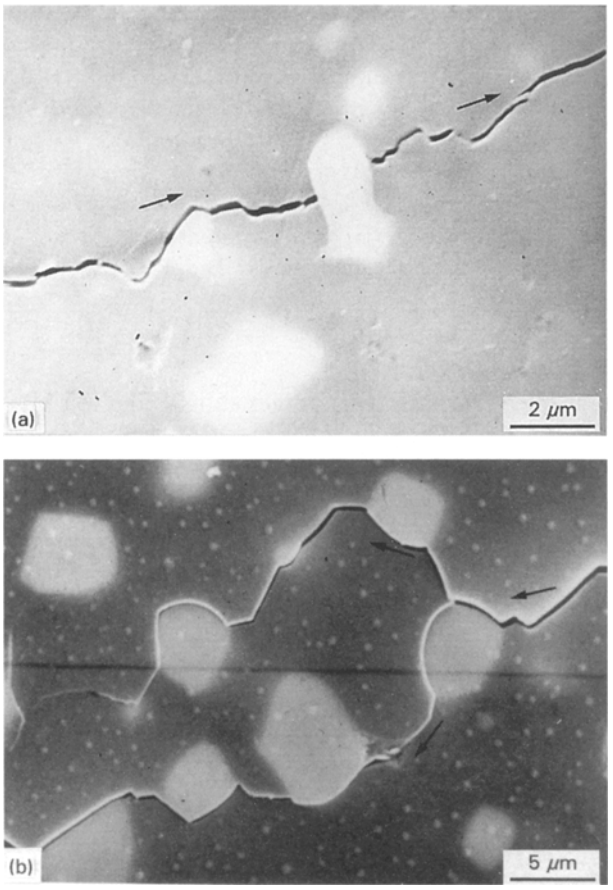

Figure 5 The interactions between Cr_3C_2 particles and microcracks induced by a Vickers' indentor (arrows indicate the direction of crack propagation) shown in polished surfaces of Al_2O_3–30 vol % Cr_3C_2 composites reinforced by (a) medium, (b) coarse, Cr_3C_2 particles.

mechanism of crack branching (as shown in Fig. 5b) is evidently an indirect result which explains the involvement of microcracking in these composites, because the occurrence of microcracking will significantly increase the number of potential sources of crack branching [15]. Thus, owing to both the microstructural observations and interactions between microcracks and Cr_3C_2 particles, the microcracking mechanism is proposed to contribute to Al_2O_3–Cr_3C_2 composites.

According to the foregoing investigations of microstructures and interactions between cracks and Cr_3C_2 particles, the possible toughening mechanisms involved in various Al_2O_3–Cr_3C_2 composites, are suggested and demonstrated in Table II. For a general and simple additive combination of these toughening processes, the overall composite toughness can be expressed by

$$K_{IC}^{C} = K_{IC}^{M} + \Delta K_{IC}^{T} \quad (4)$$

where K_{IC}^{C} is the overall toughness of composites, K_{IC}^{M} the fracture toughness contribution from the Al_2O_3 matrix, and ΔK_{IC}^{T} the sum of fracture toughness contributions from various toughening mechanisms.

For non-cubic Al_2O_3 ceramic, it has been well established that the toughness increases with increasing grain size [7, 13, 14] up to a critical grain size above

TABLE II The possible toughening mechanisms involved in different composites

Sintering temperature (°C)	Cr_3C_2 particle size (μm)	Possible toughening mechanisms[a]
1400 °C	7.5	Crack deflection (A + B/2), microcracking, crack bridging
	1.5	Crack deflection (A + B), microcracking, crack bridging
	0.5	Crack deflection (A + B), crack bridging

[a] Crack deflection (A) arises from the increase in fracture surface and change of fracture modes. Crack deflection (B) arises from the residual stress.

which spontaneous matrix microcracking and microcrack linkage degrade the toughness. However, in this case, the grain size of the Al_2O_3 matrix in composites is within the ranges 1.5–3.8 μm [19]. So, it can be reasonably defined that the fracture toughness of the matrix, K_{IC}^{M}, is constant and remains at the value of 3.8 MPa $m^{0.5}$ for all Al_2O_3–Cr_3C_2 composites in this investigation [24]. Thus, in this case, the toughness of the overall composites is completely determined by the contributions of toughening effects arising from the addition of Cr_3C_2 reinforcement ($\Delta K_{IC}^{T} = K_{IC}^{C}$). In the following discussion, it is necessary for each possible toughening mechanism to be considered.

3.2.1. Crack deflection

The first model of crack deflection proposed by Faber and Evans [3, 4], was based on a geometrical treatment of a crack deflection from its main crack plane. In this model, the toughness increase primarily arises from increasing fracture surface area and changing the fracture mode from easy mode I to the more difficult mode II or III. Based on this model, the toughness ratio ($\Delta K_{IC}^{D}/K_{IC}^{M}$) increases by 0.12 to 0.16 for uniformly distributed spherical particles with volume fractions from 0.1–0.4, respectively, as depicted in Table III. Furthermore, the toughness enhancement of crack deflection due to the additions of various Cr_3C_2 particles, can be evaluated and is also shown in Table III.

Because Faber and Evans' model ignored the local stress field at or near the interface between the matrix and second phase, at the same time, the toughness increase of crack deflection is independent of the particle size of particulate reinforcement, which is not consistent with published results. This K_{IC}^{C}/K_{IC}^{M} ratio predicted by Faber and Evans' model is always smaller than 1.4–1.8 which is typically observed in most particulate-reinforced ceramic matrix composites [25–27]. There is another toughening mechanism which is attributed to the thermal residual stress field caused by the mismatch of CTEs between the matrix and the particulates. The model proposed by Taya

et al. [8] provided the fracture toughness, K_{IC}^{C}, of a particulate composite due to the periodic residual stress field, as given by

$$K_{IC}^{C} = K_{IC}^{M} + 2q[2(\lambda - d)/\pi]^{0.5} \quad (5a)$$

$$K_{IC}^{D} = 2q[2(\lambda - d)/\pi]^{0.5} \quad (5b)$$

where K_{IC}^{M} is the critical stress intensity factor of the matrix, q the local average compressive stress in the matrix, d the average diameter of reinforcing particles, and λ the average interparticle distance. This value, λ, can be determined from [8]

$$\lambda = 1.085d/(f_P)^{1/2} \quad (6)$$

where d is the average diameter of reinforcing particles, and f_P the volume fraction of reinforcing particles.

For Al_2O_3–Cr_3C_2 composites with $\alpha_P > \alpha_m$, the average thermal stress in the particles and matrix are in tension and compression, respectively, as shown schematically in Fig. 6. The magnitude of average compressive stress, q, can be given by

$$q = 2E_m f_p(\Delta\varepsilon)/A \quad (7a)$$

$$B = (1 + \nu_m/1 - \nu_p)(E_p/E_m) \quad (7b)$$

$$A = (1 - f_p)(B + 2)(1 + \nu_m) + 3Bf_p(1 - \nu_m) \quad (7c)$$

where $\Delta\varepsilon$ is the thermal mismatch ($\sim(\alpha_p - \alpha_m)\Delta T$), E_p and E_m are the Young's modulus of Cr_3C_2 (385 GPa) [28] and Al_2O_3 (365 GPa) [21], respectively, and ν_p and ν_m are the Poisson's ratio of Cr_3C_2 (0.28) [28] and Al_2O_3 (0.254) [21], respectively.

Furthermore, consider a semi-infinite crack surrounded by a particulate-reinforced ceramic matrix composite with a thermal residual stress distribution, as shown in Fig. 6. Because the crack-tip ligament is subjected to the local average compressive stress, q, to decrease the stress intensity factor, the toughness increase due to the decrease of stress intensity factor in the matrix, can be determined from Equations 5–7 for various Al_2O_3–Cr_3C_2 composites, as shown in Table IV. Actually, the whole toughening effects of crack deflection due to Cr_3C_2 reinforcement are the sums of the above two models (Table III and Table IV).

TABLE III The increase in fracture toughness of composites predicted by Faber and Evans' model shown as functions of Cr_3C_2 content

	Reinforced particle content (vol %)			
	10	20	30	40
K_{IC}^{C}/K_{IC}^{M}	1.12	1.13	1.15	1.16
ΔK_{IC}^{0} (MPa m$^{0.5}$)	0.46	0.49	0.57	0.61

3.2.2. Microcracking

The phenomenon of microcrack toughening was postulated more than a decade ago [10–12]. The general concept of microcrack toughening is of a shielding at the crack tip formed by microcracking in a brittle solid. There is a hysteresis of the elemental stress–strain curve or crack branching, which lead to the absorption of extra energy from the applied loads. Therefore, microcracking can provide an opportunity for an extreme increase in fracture toughness. Furthermore, the toughening effect of penny-shaped microcracks is described by [12]

$$\Delta K_{IC}^{T}/K_{IC}^{M} = 1.42\Omega \quad (8)$$

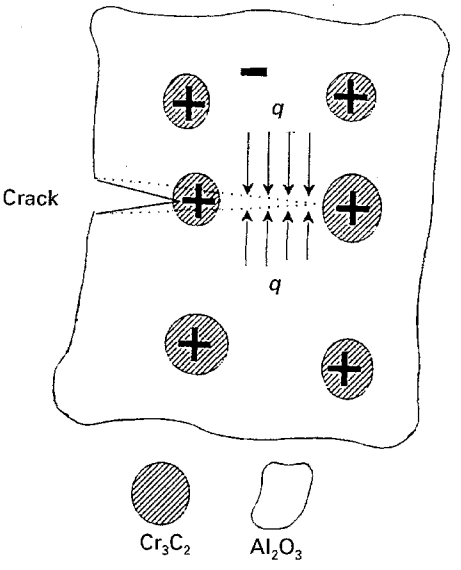

Figure 6 A schematic diagram demonstrating that the residual compressive stress, q, in Al_2O_3 can reduce the stress intensity factor of the crack tip. +, Residual tensile stress; −, residual compressive stress.

TABLE IV The increase of fracture toughness owing to the presence of residual compressive stress to decrease the stress intensity factor at the crack tip, shown as functions of Cr_3C_2 content and particle size

Cr_3C_2 content (vol %)	Particle size (μm)											
	7.5				1.5				0.5			
	10	20	30	40	10	20	30	40	10	20	30	40
λ (μm)	25.4	18.2	14.8	12.9	5.15	3.64	2.97	2.58	1.72	1.22	1.0	0.86
A	6.3	6.36	6.4	6.45	6.3	6.36	6.4	6.45	6.3	6.36	6.4	6.45
B	3	3	3	3	3	3	3	3	3	3	3	3
q(MPa)	138	273	407	539	138	273	407	539	138	273	407	539
ΔK(MPa m$^{0.5}$)	0.94	1.43	1.76	1.99	0.42	0.64	0.79	0.89	0.24	0.37	0.46	0.52

where $\Omega = N < R^3 >$ is the number density of microcracked particles, with N being the number of microcracked particles per unit volume and as functions of particle radius. For Al_2O_3–Cr_3C_2 composites reinforced with coarse and medium Cr_3C_2 particles, the microcracks formed either spontaneously or stress-induced, are frequently observed at the interfaces. No doubt the density of microcracked particles, N, can be supposed to be equivalent to the value of the volume content of Cr_3C_2 especially at high Cr_3C_2 content. However, the toughening effect of microcracks is not involved in the composites reinforced by fine Cr_3C_2 particles, due to the fact that the fine Cr_3C_2 particle is much smaller than that of the critical particle size (3.2 μm). Furthermore, the toughening effect contribution from microcracking can be evaluated from Equation 8 and is indicated in Table V.

3.2.3. Crack bridging

The basic toughening mechanism of crack bridging in a brittle matrix due to dispersed particulate reinforcements, is similar to that of the fibre or whisker-reinforced ceramics. As the existing crack front may propagate in the brittle matrix and encounter particulate reinforcement, the crack front will encircle the unbroken particulate due to weak interfacial bonding and become approximately a macroscopic planar crack perpendicular to the applied stress. In the resulting configuration, the particulates behind the crack tip can act as bridges between the opposing faces of the crack to prevent excessive crack opening and thereby reduce the crack driving force or the stress intensity factor, K_1, at the crack tip. Because K_1 must reach a critical value, K_{IC}, for further crack extension, this requires a higher value of applied stress for crack propagation than that necessary in the absence of particulates. Furthermore, for brittle particulate-reinforced ceramic composites, the crack-bridging contribution to the toughness, ΔK_{IC}^{B}, which was proposed by Becher [7], is

$$\Delta K_{IC}^{B} = (A^{B}\tau^{B}DE^{B}/2)^{0.5} \quad (9)$$

where A^B is the fraction of bridging grains, which is supposed to be equal to the Cr_3C_2 volume content of composites, τ^B the bridging frictional stress at the interface which is around 30 MPa [12] in the absence of chemical reactions at interface, E^B the Young's modulus of the bridging grain ($E^B = 385$ GPa), and D the debonding length of the bridging grain which is equal to half the diameter of the bridging grain.

Owing to the absence of rupture of Cr_3C_2 during the fracturing processes, it is noted that there are two main factors of crack bridging which are beneficial to the toughness of composites. In addition to the fracture energy being used to create a new fracture surface at the debonding interfaces, the frictional bridging can significantly enhance the fracture resistance of the composites. The toughness contributed from crack bridging for various Al_2O_3–Cr_3C_2 composites, can be determined, as shown in Table VI.

For comparison of the various composites, the individual toughening effects contributed from the aforementioned toughening mechanisms are rearranged and demonstrated in Figs 7–9. Fig. 7 shows the superimposed contributions predicted from crack-deflection and crack-bridging mechanisms for Al_2O_3–Cr_3C_2 composites reinforced by fine Cr_3C_2 particles. Evidently, the total predicted toughness enhancement is close to the experimental results for Al_2O_3–Cr_3C_2 (S) composites with 10–40 vol % Cr_3C_2 (S) content. However, there is some distinction between the experimental results and the predicted toughening effects, especially in high Cr_3C_2 content of Al_2O_3–Cr_3C_2 (M) composites, as indicated in Fig. 8. Similarly, for Al_2O_3–Cr_3C_2 (L) composites (Fig. 9), the toughening contribution of crack-bridging is gradually diminished with increasing Cr_3C_2 content of the composites. A possible reason is the presence of microcracks leading to the extensive reductions of bridging stress and fracture energy of debonding [6]. Because the microcracking density increases with Cr_3C_2 content of composites reinforced by medium or coarse Cr_3C_2 particles, a greater deviation between the experimental results and the predicted overall toughness can be obtained as the Cr_3C_2 content of the composites become higher. Therefore, the addition of coarse Cr_3C_2 particles is more effective in the toughening of the Al_2O_3 matrix. The toughening effects are mainly contributed from the crack-deflection and microcracking mechanisms. However, the toughening contributions of composites reinforced by fine Cr_3C_2 particles are primarily generated from crack-deflection and crack-bridging mechanisms.

TABLE V The toughening effects contribution from the microcracking for Al_2O_3–Cr_3C_2 composites

Cr_3C_2 particle size (μm)	Cr_3C_2 content (vol %)	ΔK_{IC}^{M} (MPa $m^{0.5}$)
7.5	10	0.54
	20	1.08
	30	1.62
	40	2.2
1.5	10	0.54
	20	1.08
	30	1.62
	40	2.2

TABLE VI The toughening increase contribution from the crack bridging for various Al_2O_3–Cr_3C_2 composites

Cr_3C_2 content (vol %)	Toughening increase (MPa $m^{0.5}$) for Cr_3C_2 particle sizes (μm)		
	7.5 μm	1.5 μm	0.5 μm
10	1.97	0.90	0.51
20	2.70	1.24	0.71
30	3.43	1.58	0.89
40	3.94	1.80	1.41

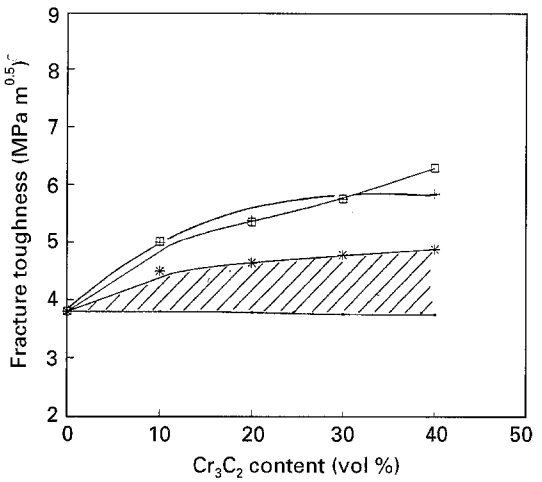

Figure 7 Comparison of experimental results with the total toughening contributions from crack deflection (CD), and crack bridging (CB) for Al_2O_3–Cr_3C_2 (S) composites hot-pressed at 1400 °C, shown as a function of Cr_3C_2 content. (■) Al_2O_3, (+) Exp. S, (*) CD ($K1$), (□) CB ($K2 + K1$).

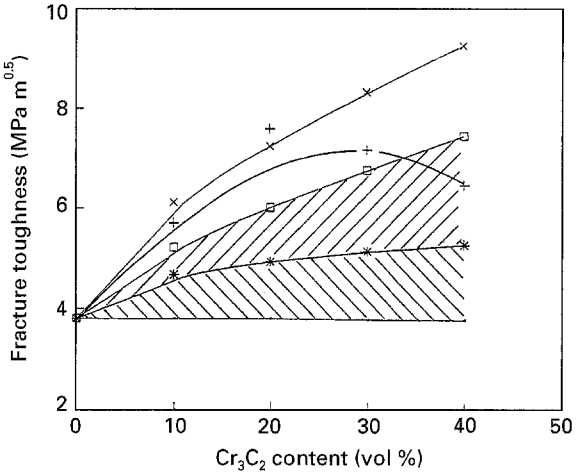

Figure 8 Comparison of experimental results with the total toughening contributions from crack deflection (CD), crack bridging (CB), as well as microcracking (MC) for Al_2O_3–Cr_3C_2 (M) composites hot-pressed at 1400 °C, depicted as a function of Cr_3C_2 content. (■) Al_2O_3, (+) exp. M, (*) CD ($K1$), (□) MC ($K2 + K1$), CB ($K3 + K2 + K1$).

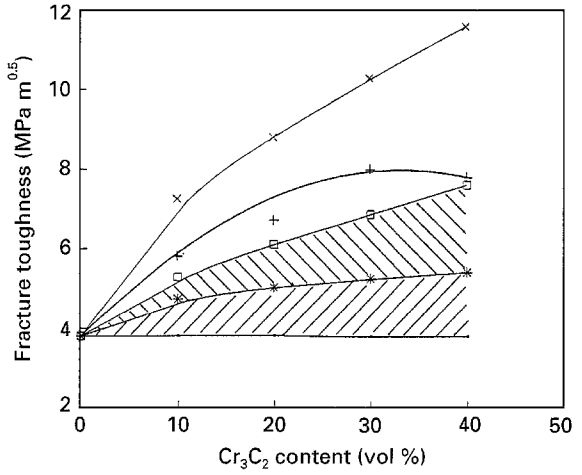

Figure 9 Comparison of experimental results with the total toughening contributions from crack deflection (CD), crack bridging (CB), and microcracking (MC) for Al_2O_3–Cr_3C_2 (L) composites hot-pressed at 1400 °C, illustrated as a function of Cr_3C_2 (■) Al_2O_3, (+) exp. L, (*) CD ($K1$), (□) MC ($K2 + K1$), (×) $K1 + K2 + K3$.

4. Conclusion

The addition of coarse and medium Cr_3C_2 particles to the Al_2O_3 matrix can give rise to penny-shaped microcracks, which result from the mismatch of TECs between Al_2O_3 and Cr_3C_2, in the Al_2O_3/Cr_3C_2 interfaces. The critical volume of spontaneous microcracks is 10 and 30 vol % for coarse (7.5 μm) and medium (1.5 μm) Cr_3C_2 particles, respectively, while, there is absence of spontaneous microcracks in composites reinforced by fine Cr_3C_2 (0.5 μm) particles. The incorporation of coarse Cr_3C_2 particles is more effective in toughening Al_2O_3 than that of fine Cr_3C_2 particles. The toughening effect is mainly contributed from crack deflection and microcracking. Otherwise, the primary toughening mechanisms for composites incorporating fine Cr_3C_2 particles are crack bridging and crack deflection.

Acknowledgement

The authors acknowledge the financial support from the Ministry of Economic Affairs of Taiwan under contract Mat.3AB3210.

Reference

1. F. F. LANGE, *Philos. Mag.* **179** (1970) 983.
2. A. G. EVANS, *ibid.* **1372** (1972) 26.
3. K. T. FABER and A. G. EVANS, *Acta. Metall.* **31** (1983) 565.
4. *Idem, ibid.* **31** (1983) 577.
5. B. B. BUDIANSKY, J. C. AMAZIGO and A. G. EVANS, *J. Mech. Phys. Solids* **36** (1988) 167.
6. F. ERDOGAN and P. F. JOSEPH, *J. Am. Ceram. Soc.* **72** (1989) 262.
7. P. F. BECHER, *ibid.* **74** (1991) 255.
8. M. TAYA, S. HAYASHI, A. S. KABAYASHI and H. S. YOON, *ibid.* **73** (1990) 1382.
9. A. V. VIRKAR and D. L. JOHNSON, *ibid.* **60** (1977) 514.
10. K. T. FABER and A. G. EVANS, *ibid.* **64** (1981) 394.
11. J. W. HUTCHINSON, *Acta Metall* **35** (1987) 1605.
12. A. G. EVANS, *J. Am. Ceram. Soc.* **73** (1990) 187.
13. P. F. BECHER, C. H. HSUEH, P. ANGELINI and T. N. TIEGS, *ibid.* **71** (1988) 1050.
14. P. L. SWANSON, C. J. FAIRBANKS, B. R. LAWN, Y. MAI and B. J. HOCKEY, *ibid.* **70** (1987) 279.
15. R. W. RICE, *Ceram. Eng. Sci. Proc.* **11** (1990) 667.
16. *Idem, ibid.* **2** (1981) 661.
17. S. T. BULJAN, A. E. PASTO and H. J. KIM, *Am. Ceram. Soc. Bull.* **68** (1989) 387.
18. R. W. DAVIDGE, in "Fracture Mechanics of Ceramics", Vol. 4, edited by R. C. Bradt, D. P. H. Hasselman and F. F. Lange (Plenum Press, New York, 1978) pp. 447–67.
19. C. T. FU, A. K. LI and J. M. WU, *J. Mater. Sci.* **28** (1993) 2671.
20. *Idem, ibid.* **28** (1993) 6285.
21. W. D. KINGERY, H. K. BOWEN and D. R. VHLMANN, in "Introduction to Ceramics", (Wiley, New York, 1976) p. 785.
22. K. TSUKUMA, K. UEDA and M. SHIMEDA, *J. Am. Ceram. Soc.* **68** (1985) C4, C5.
23. Y. S. CHOU and D. J. GREEN, *ibid.* **76** (1993) 1452.
24. R. W. RICE, S. W. FREIMAN and P. F. BECHER, *ibid.* **64** (1981) 345.
25. M. G. JENKINS, J. A. SALEM and S. G. SESHADRI, *J. Compos. Mater.* **23** (1989) 77.
26. M. A. JANNEY, *Am. Ceram. Soc. Bull* **66** (1987) 322.
27. C. H. McMURTRY, W. D. G. BOECKER, S. G. SESHADRI, J. S. ZANGHI and J. E. GARNIER, *ibid.* **66** (1987) 325.
28. L. E. TOTH, in "Transition Metal Carbides and Nitrides" (Academic Press, New York, 1971) pp. 141–84.

Received 19 April 1994
and accepted 13 February 1996